Published version available at: https://doi.org/10.1016/j.combustflame.2022.112109

Asymptotic study of premixed flames in inert porous media layers of finite width: parametric analysis of heat recirculation phenomena

Vadim N. Kurdyumov[1], **Daniel Fernández-Galisteo, Carmen Jiménez**

Department of Energy, CIEMAT, Avda. Complutense 40, 28040 Madrid, Spain

Abstract

In this paper, we present an investigation on super-adiabatic premixed flames in an inert porous medium layer of finite length. The combustion process is modeled by a one-step Arrhenius kinetics in which density variations are taken into account. The asymptotic case of large ratio of thermal conductivities of solid to gas phases and the high activation energy limit are explored. The results obtained for these limiting cases are compared to those for finite values of these parameters. The use of the flame sheet model allows us to obtain steady-state solutions in an analytical form thus facilitating the parametric analysis.

The investigation focuses on the phenomenon of multiplicity of steady-state solutions. It is shown that two or three (nontrivial) steady-state solutions are possible, depending on the flow rate intensity. The critical values of the parameters for the existence of multiple solutions are also determined. The stability of the obtained solutions is finally investigated by means of time-dependent simulations.

1 Introduction

Although the fundamental ideas related to super adiabatic combustion have more than fifty years of history [1–3], attention to this topic is not waning, but only increasing. A key characteristic of these devices is the ability to achieve a temperature in the combustion zone that exceeds the temperature obtained from a simple enthalpy balance between the initial mixture composition and the final products. This makes it possible to use them for various purposes. Among them, one can list the after burning of harmful impurities in gases for their final disposal or the extraction of electrical energy from a micro-combustion device in conditions of remoteness from other sources of energy. Detailed reviews of these micro-combustion devices and their applications can be found in multiple publications, see [4–11].

[1]Corresponding author

A typical design used for micro combustion devices is a system of channels in which flows are established in a countercurrent pattern in adjacent channels. The width of the channels should be comparable to the thermal width of the flame, which is necessary to ensure enough heat transfer between the channels. This makes it possible to enhance the effect of heat recirculation, by which part of the heat energy does not leave the system and is used to preheat the incoming fresh mixture.

Another way for organizing heat recirculation is the use of an inert porous medium to increase the heat exchange between the hot combustion products and the cold mixture entering the device. In this case, the requirement of narrow channel width disappears, which obviously reduces the restrictions on the maximum values of the flow rate through the device.

The interaction of premixed flames with inert porous media has been studied in several investigations applying asymptotic, numerical and analytical methods. Four different configurations can be identified in these studies, depending on the porous medium geometry, the flow direction and the flame position. In the first configuration [12, 13], the porous layer was assumed to be semi-infinite, and fresh combustible gas was supplied from the gaseous half-space. In this configuration combustion takes place inside the porous medium at a finite distance from the gas-porous layer boundary and a single steady flame position exists.

In [14–17], the structure of a flame motionless relative to an infinite inert porous medium was investigated. This state corresponds to a unique, particular value of the filtration velocity of the incoming gas. In all the cases mentioned above [12–17] the maximum temperature in the flame exceeds the adiabatic flame temperature value.

In [18–21], the studied configuration was that of a premixed flame in a gas flow emerging from a semi-infinite porous media with a fixed (cold) temperature. In this case the flame is located at a finite distance downstream from the porous layer edge. It was shown that the thermal interaction of the flame with the upstream porous layer can promote oscillatory dynamics even for flames with unity Lewis number.

In the last configuration, the flame structure inside a porous layer of finite length was studied, see [17, 22–24]. Contrary to the previous situation, the temperature of the porous layer is not fixed and it has to be found as a part of the solution. In this configuration, two steady-state solutions with two different flame positions situated inside the porous layer were identified. These studies were also carried out using asymptotic [22], numerical [23, 24] and analytical methods [17]. Interestingly, in [17] where the configurations with finite and infinite porous layer width were considered, it was shown that there is a maximum length above which the finite

length layer is equivalent to an infinite layer from the point of view of the efficiency of the recirculation.

The present investigation revisits the last configuration and considers the structure, stability and dynamics of a flame in an inert porous layer of finite length. Anticipating the presentation of the results, and also in order to emphasize the novelty of the present study, we indicate that in addition to the two solutions reported previously, the existence of a third possible flame mode is predicted for certain values of the parameters. Additionally, we investigate the stability of the steady state solutions, which, to the best of our knowledge, has not been studied before, and demonstrate that two of the three modes are stable.

It is interesting to note that a similar pattern with two stable steady-states was reported recently in [25], where a porous burner of a different and more complex type was studied experimentally. Nevertheless, the presented work does not set the task of modeling this type of burners, which would require a particular investigation.

The analysis is carried out under the physical assumption that the value of the thermal conductivity of the solid phase is much higher than the thermal conductivity of the gas. The steady-state analysis is carried out in an analytical form under the natural assumption for combustion of a high activation energy. It should be noted that in the previous studies (with the exception of [24]) the assumption of a constant gas density was adopted. Unlike this, changes in gas density with temperature which affect the reaction rate are taken into account in the present study. The obtained asymptotic results are compared with the numerical solutions for finite values of these parameters.

The aim of this work is not to study a specific case, but rather to explore general trends in the structure of a flame stabilized in a porous medium of finite length from an asymptotic point of view. The article is structured as follows. Section 2 presents the mathematical formulation of the problem. The asymptotic assumptions adopted in the study are discussed in Section 3, where the corresponding analytical solution to the problem is also constructed. Section 4 describes the solution to the problem for finite values of the Zel'dovich number, which is then compared with the analytical solution. Section 5 is devoted to a discussion of the results.

2 General formulation

Consider a combustible gaseous mixture at initial temperature T_0, density ρ_0, and fuel mass fraction Y_0 flowing through an inert porous layer of finite width L. The gas velocity far upstream

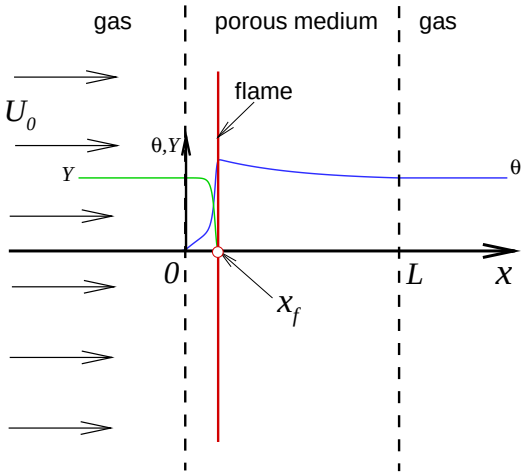

Figure 1: Sketch of the problem.

the porous layer is U_0. The configuration sketch is shown in Fig. 1. Following the standard continuum model for a porous medium (see [26], for example), we denote as U the gas seepage velocity inside the porous medium and the gas velocity outside the porous layer. This magnitude ensures the continuity of the gas mass flow rate, ρU, through the gas-porous medium boundary. Inside the porous layer, a two-temperature continuous model is used, in which T and T_s denote the temperatures of the gas and the solid phase, respectively. It is assumed that the motion is spatially one-dimensional and all variables are functions of a single spatial coordinate x and time t.

The combustible mixture undergoes a chemical reaction modeled by a global irreversible step $\mathrm{F} + \mathrm{O} \rightarrow \mathrm{P}$, where F, O and P denote the fuel, the oxidizer and the products, respectively. Assuming that the mixture is lean in fuel, the oxidizer mass fraction remains nearly constant. Generalization of the problem to cases of non-lean mixtures will be done somewhere else. The amount of fuel consumed per unit volume of gas and per unit time is given by $\Omega = \mathcal{B}\rho^n Y \exp(-\mathcal{E}/\mathcal{R}_g T)$, where $\mathcal{B}$ is a pre-exponential factor, ρ is the density of the mixture, Y is the fuel mass fraction, $\mathcal{E}$ is the overall activation energy and $\mathcal{R}_g$ is the universal gas constant. The Arrhenius kinetics frequently used to simulate a combustion process is a simplification of more complex multicomponent kinetics. There is no unanimous agreement in the combustion literature concerning the power n, and values 0, 1 and 2 for n have been used used in different studies. Formally, $n = 0$ corresponds to the diffusion-thermal approxi-

mation when density changes are neglected. If we consider in a simplified way the process of a binary chemical reaction, when one fuel molecule meets one oxidizer molecule, the collision frequency should be proportional to the concentrations of each mixture component at a given point of space. Thus, perhaps the most reasonable compromise is index $n = 2$.

For simplicity, we will assume constant values for the constant-pressure gas and solid heat capacities, c_g and c_s, the conductivities, λ_g and λ_s, the mass fuel diffusion coefficient, $\rho\mathcal{D}$, the solid phase density, ρ_s, as well as the isobaric assumption. While some research has been done relaxing this assumption, it will be reported elsewhere in order not to overwhelm the presentation. Here, we can report that taking into account variable properties leads only to relatively small changes in the quantitative results without changing the qualitative behavior of the curves.

The porosity of the layer is denoted as ϕ hereinafter. Although this value for porous ceramic materials is about $0.6 \div 0.8$, in this study a wider range for porosity is considered, $\phi = 0.4 \div 0.8$. Heat exchange between the gas and solid phases follows a linear law, namely, the amount of energy that is transferred from one phase to another per unit volume and per unit time is proportional to the temperature difference, $H_v(T - T_s)$. There is an experimental correlation estimate suggested in [30] for the coefficient of volumetric heat transfer, H_v, between phases:

$$\frac{H_v d_p^2}{\lambda_g} = \left(0.0426 + \frac{1.236}{L/d_p}\right) Re_d \,, \tag{1}$$

where d_p is the characteristic pore size and $Re_d = \rho u d_p/\phi\mu$, with μ the viscosity. According to [30], this correlation formula is valid in the interval $2 < Re_d < 836$. The same expression was used in the numerical studies presented in [24]. Although Eq. (1) can raise questions, since it includes the layer length L (the global characteristic) to correlate the local characteristic of the process (at a given point in space), and also does not include the thermophysical properties of the porous material, it will be used here to estimate the coefficient of volumetric heat transfer between phases. In the present study, this value is taken constant when carrying out parametric analysis. Anticipating the analytical procedure to be developed, a generalization to account for the flow-rate dependence for this quantity can be easily made.

When selecting characteristic scales for a combustion problem, it is convenient to use the characteristic values corresponding to a planar adiabatic flame for a given mixture composition. In the following, the burning velocity of the planar (gaseous) flame S_L, the thermal flame thickness defined as $\delta_T = \mathcal{D}_T/S_L$, with $\mathcal{D}_T = \lambda_g/\rho_0 c_g$ the thermal diffusivity, and the adiabatic flame temperature $T_a = T_0 + QY_0/c_g$, with Q the total heat of combustion per unit mass of fuel, are used to specify the non-dimensional parameters. Non-dimensional temperatures defined as

$\theta = (T - T_0)/(T_a - T_0)$ and $\theta_s = (T_s - T_0)/(T_a - T_0)$ are introduced in the following, while S_L, Y_0 and ρ_0 are used to normalize the velocity, the fuel mass fraction and the density, respectively.

Let's introduce the following functions

$$\Phi(x) = \begin{cases} \phi, & 0 \leqslant x \leqslant \ell\,, \\ 1, & x < 0,\ x > \ell\,, \end{cases} \quad B(x) = \begin{cases} b, & 0 \leqslant x \leqslant \ell\,, \\ 0, & x < 0,\ x > \ell\,, \end{cases} \tag{2}$$

where ϕ represents the porous layer porosity and b is the dimensionless effective heat transfer coefficient between the gas and solid phases, defined as a function of H_v further below. In what follows, a two-temperature continuum model similar to that used, for example, in [14–16] is applied.

It is well known that possible heat losses with the external environment can affect the overall map of possible solutions. Accounting for these effects requires taking into account some additional geometric characteristics of the burner, such as, for example, the transverse width of the porous layer. For the sake of simplicity, heat losses will be assumed to be negligible in the present study. This reduces the number of parameters thus facilitating the obtention of more general results within a simplified model.

The well-known conservation equations of the mass, the fuel mass and the gas thermal energy for both a space occupied by a porous medium ($\Phi = \phi$) and a porous-free space ($\Phi = 1$) are written in the form

$$\Phi \frac{\partial \rho}{\partial t} + \frac{\partial (\rho u)}{\partial x} = 0\,, \tag{3}$$

$$\Phi \rho \frac{\partial Y}{\partial t} + \rho u \frac{\partial Y}{\partial x} = \frac{1}{Le} \frac{\partial}{\partial x} \left(\Phi \frac{\partial Y}{\partial x} \right) - \Phi\, \omega\,, \tag{4}$$

$$\Phi \rho \frac{\partial \theta}{\partial t} + \rho u \frac{\partial \theta}{\partial x} = \frac{\partial}{\partial x} \left(\Phi \frac{\partial \theta}{\partial x} \right) + \Phi\, \omega - B(\theta - \theta_s)\,. \tag{5}$$

These equations are considered for $-\infty < x < \infty$. The corresponding equation for the solid thermal energy becomes

$$(1 - \phi) \xi \frac{\partial \theta_s}{\partial t} = (1 - \phi) \Lambda \frac{\partial^2 \theta_s}{\partial x^2} + b(\theta - \theta_s)\,, \tag{6}$$

considered for $0 < x < \ell$. The above equations are supplemented by the isobaric equation of state for the (ideal) gas

$$\rho(1 + q\theta) = 1\,. \tag{7}$$

The dimensionless reaction rate is written as

$$\omega = \frac{\beta^2}{2Le\, u_p^2} (1 + q)^n \rho^n Y \exp \left\{ \frac{\beta(\theta - 1)}{1 + q(\theta - 1)/(1 + q)} \right\}. \tag{8}$$

The boundary conditions for the velocity, the gas density, the temperature and the fuel mass fraction are described by fixing quantities far upstream and applying weak conditions far downstream

$$\begin{aligned} x \to -\infty: &\quad u - m = \rho - 1 = Y - 1 = \theta = 0; \\ x \to \infty: &\quad \partial Y/\partial x = \partial\theta/\partial x = 0\,. \end{aligned} \tag{9}$$

The conditions at the planes separating the porous layer and gas situated at $x = 0$ and $x = \ell$ are expressed in the form of the continuity of the mass fraction and the gas phase temperature together with their diffusion fluxes as follows

$$x = 0,\ \ell: \quad [Y] = [\theta] = [\Phi\,\partial Y/\partial x] = [\Phi\,\partial\theta/\partial x] = 0\,, \tag{10}$$

where $[f] = f(x^+) - f(x^-)$. For the solid phase temperature we assume that

$$x = 0,\ \ell: \quad \partial\theta_s/\partial x = 0\,, \tag{11}$$

thus neglecting, for simplicity, the radiation-thermal effects from the porous surfaces.

The following parameters appear in the above equations: the dimensionless flow rate, $m = U_0/S_L$, the dimensionless length of the porous layer, $\ell = L/\delta_T$, the Zeldovich number, $\beta = \mathcal{E}(T_a - T_0)/\mathcal{R}_g T_a^2$, the Lewis number, $Le = \lambda_g/c_p\rho_0\mathcal{D}$, the heat release parameter, $q = (T_a - T_0)/T_0 = Q\,Y_0/c_p\,T_0$, the dimensionless heat-exchange parameter, $b = H_v\delta_T/\rho_0 c_g S_L$, the ratio of thermal conductivities, $\Lambda = \lambda_s/\lambda_g$, and the ratio of the mass-weighted heat capacities of the solid and gas phases, $\xi = \rho_s c_s/\rho_0 c_g$. One can see that for steady-state solutions, when $\partial/\partial t \equiv 0$ is assumed, the value of ξ becomes irrelevant.

In theoretical studies related to combustion, the Zel'dovich number, β, is often used as a large parameter in asymptotic expansions, while the other parameters are assumed (formally) to be of the order of unity. It should be noted that in fact β and the heat release parameter, q, are related as $\beta = \mathcal{N}\,q/(1+q)^2$, where $\mathcal{N} = \mathcal{E}/\mathcal{R}_g T_0$ is the dimensionless activation energy based on the initial temperature of the mixture. In what follows, we will use both quantities to characterize the flame, and the value $\beta = 10$ will be used as a reference one corresponding to $\mathcal{N} = 72$ for $q = 5$. These values are standard in combustion modeling.

To estimate the dimensionless heat transfer coefficient between phases, b, we will assume that $L \gg d_p$. In this case, it follows from Eq (1) that $b = 0.0426\,Re_d\,\delta_T^2/d_p^2$. Thus, reasonable values for b are in the range $0.03 \div 0.3$. The specific value depends on the material of the porous layer and the composition of the combustible mixture. In this study, the value $b = 0.2$ is chosen as a reference value.

The factor $u_p = S_L/S_L^{as}$ included in Eq. (8) ensures that the non-dimensional speed of a planar adiabatic gaseous flame is equal to unity for a given finite value of β. Here S_L^{as} is the asymptotic value of adiabatic laminar flame speed calculated at $\beta \to \infty$:

$$S_L^{as} = \sqrt{2(\lambda_0/c_p)Le\beta^{-2}\mathcal{B}\rho_0^{n-2}(T_0/T_a)^{\,n}}\exp(-\mathcal{E}/2\mathcal{R}T_a)$$

Precise calculation of u_p requires the solution of the following eigenvalue problem

$$\begin{aligned} &d\theta/dz = d^2\theta/dz^2 + \omega, \quad dY/dz = Le^{-1}d^2Y/dz^2 - \omega, \\ &z \to -\infty: \quad \theta = Y - 1 = 0, \quad z \to +\infty: \quad \theta - 1 = Y = 0, \end{aligned} \tag{12}$$

where ω is given by Eq. (8). For large β the eigen-value of Eq. (12) is of the form

$$S_L/S_L^{as} = 1 + c_1(Le, q, n)/\beta + O(\beta^{-2}) + \ldots,$$

see [31]. When carrying out the asymptotic analysis for $\beta \gg 1$ in the following sections, this value is equal to unity, in the leading approximation. However, when performing numerical calculations at finite β values, u_p is computed numerically by a shooting method.

The use of the factor u_p makes it possible to generalize the results to more complex kinetics. Indeed, for this it is only necessary to use the speed of a planar adiabatic combustion wave (e.g. measured experimentally) and the adiabatic flame temperature (obtained from the balance of enthalpy of the initial and final products) in writing the dimensionless parameters.

The flame position, x_f, is determined by the point at which the reaction rate reaches its maximum value, $\omega|_{x=x_f} = \omega_{max}$. From a general consideration of the governing equations, it can be obtained that for steady-state solutions the gas temperature far downstream is equal to the adiabatic one, $\theta(x \to \infty) = 1$. This trivial fact also follows from the energy conservation law in the absence of heat loss.

3 Asymptotic analysis

3.1 Limit $\Lambda \gg 1$

The dimensional parameters describing the properties of the gas and solid phases differ by orders of magnitude. Typical magnitudes of thermal conductivities suggest $\Lambda = \lambda_s/\lambda_g = O(10^3)$. Thus, the limit of $\Lambda \to \infty$ is considered below. Assuming (formally) that all remaining parameters are of order unity, we expand θ_s in the form $\theta_s = \theta_s^{(0)} + \Lambda^{-1}\theta_s^{(1)} + \ldots$. To the leading

order, Eq. (6) is reduced to $\partial^2\theta_s^{(0)}/\partial x^2 = 0$. The boundary conditions given by Eq. (11) indicate that $\theta_s^{(0)}$ is a function of time only. After integrating Eq. (6) over the porous layer thickness and dropping the superscript, we have

$$(1-\phi)\,\xi\frac{d\theta_s}{dt} = b\cdot\left(\frac{1}{\ell}\int\limits_0^\ell \theta dx - \theta_s\right). \tag{13}$$

A similar limit of the constant temperature of a porous medium was considered in [23], where the balance for this value was established by heating from the outside. The results obtained for $\Lambda \gg 1$ are compared below with those for finite ratios of the thermal conductivities.

3.2 Limit $\beta \gg 1$

The typical Zel'dovich number is large, $\beta \gg 1$, leading to a narrow combustion zone, of order δ_T/β, within which $\omega > 0$. The standard treatment consists in replacing the spatially distributed kinetics given by Eq. (8) by an infinitely thin flame sheet,

$$\omega = F(\theta_f, G)\cdot\delta(x - x_f)\,, \tag{14}$$

where $\delta(\cdot)$ is the Dirac δ-function, $G = -d\theta/dx|_{x=x_f+}$ denotes the temperature gradient just behind the flame sheet (at the burnt side) and θ_f is the flame temperature. The substantiation of this procedure should be referred to [31] where the method of matched asymptotic expansions was first applied to the problem of steady-state propagation of an adiabatic planar combustion wave. In that case $\theta_f = 1$ and $G = 0$. The rigorous justification for this approximation for general unsteady cases ($G \neq 0$) was suggested in [27]. In the recent study [28] an extension was made for transport properties variable with temperature and heat-losses. This δ-function approximation has been used many times in the past, mainly for analytical purposes.

An asymptotic analysis based on the method of matched asymptotic expansions gives

$$F(\theta_f, G) = \mu(G)^{-1/2}\left(\frac{1+q\theta_f}{1+q}\right)^{2-n/2}\cdot\exp\left\{\frac{\beta}{2}\frac{(\theta_f-1)}{(1+q\theta_f)/(1+q)}\right\}, \tag{15}$$

see [27, 28]. The value of μ in Eq. (15) is determined by considering the inner flame region. It leads to the classical problem first investigated by Liñán in his pioneering asymptotic study of diffusion flames [29]. Finally, the dependence of μ on G can be approximated as $\mu \approx 1 - \mu_1 G$, where $\mu_1 = 1.344046$ was calculated numerically.

Anticipating the comparison of the results of asymptotic analysis with the results of numerical calculations with the spatially distributed kinetics, we can conclude that the effect of a nonzero value of G is relatively small. Thus, the choice $\mu \equiv 1$ is made in present study leading to $F = F(\theta_f)$ in Eq. (15).

When considering an infinitely thin inner combustion region, the fuel mass fraction and temperatures must be continuous at the flame sheet,

$$[Y]_{x=x_f} = 0, \quad \theta|_{x_f-} = \theta|_{x_f+} = \theta_f. \tag{16}$$

Integrating Eqs. (4)-(5) across $x = x_f$ gives the well-known jump conditions

$$Le^{-1}[dY/dx]_{x=x_f} = F(\theta_f), \quad [d\theta/dx]_{x=x_f} + Le^{-1}[dY/dx]_{x=x_f} = 0. \tag{17}$$

For the temperature of the solid phase, integration of Eq. (6) around $x = x_f$ leads to

$$[\theta_s]_{x=x_f} = [d\theta_s/dx]_{x=x_f} = 0\,. \tag{18}$$

Obviously, Eq. (18) is satisfied automatically for cases with $\Lambda \gg 1$.

3.3 Steady-state asymptotic solutions

Consider steady-state solutions imposing $\partial/\partial t \equiv 0$ in Eqs. (3)-(6). Eq. (3) leads to $\rho u = m$ satisfied everywhere. Thus, for time-independent solutions, the density changes affect only the reaction rate term given by Eq. (8), where ρ^n is a factor. It should be also noted that steady-state solutions are independent of the parameter ξ appearing as a factor in front of the time derivative.

Let us assume that $0 < x_f < \ell$. Consideration of the inner flame region by means of the matched asymptotic expansions method shows that the fuel leakage (mass fraction of unburned fuel behind the flame) is, at least, of the order of β^{-1}. This effect is small in the first approximation. Thus, $Y = 0$ can be imposed behind the flame, for $x > x_f$, and the steady-state solution of Eq. (4) is

$$Y = \begin{cases} 1 - \exp\{mLe(x - x_f/\phi)\}, & x < 0\,, \\ 1 - \exp\{mLe(x - x_f)/\phi\}, & 0 < x < x_f\,. \\ 0, & x > x_f. \end{cases} \tag{19}$$

Here the continuity of the mass fraction and its diffusion flux has been required at $x = 0$.

From Eqs. (17) and (19) it follows, that

$$m = \phi \cdot F(\theta_f)\,. \tag{20}$$

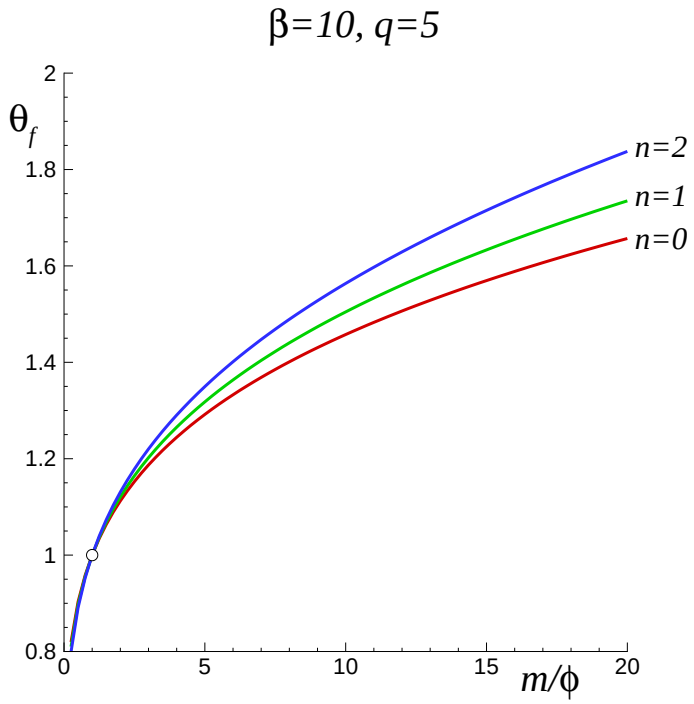

Figure 2: Dependence of the flame temperature θ_f on m/ϕ given by Eq. (21) for different n, for $\beta = 10$, $q = 5$.

The same result can be obtained by integrating Eq. (4) over x within $\pm\infty$. It should be noted that this relation is obtained only if the flame sheet is either inside the porous layer, where $\phi < 1$, or outside it, where $\phi = 1$. The case when the position of the flame coincides with the boundary of the porous layer, for $x_f = 0$ or $x_f = \ell$, should be considered separately. This situation is discussed in the Appendix.

Equation (20) provides a direct relation between the flame temperature, θ_f, and the flow rate, m. Note that the function F is a monotonically increasing function of the flame temperature θ_f. This means that at a fixed value of m, a decrease in ϕ leads to an increase in the flame temperature. Finally, the flame temperature can be expressed as

$$\theta_f = \frac{\beta(1+q)^2 - q(4-n)Z}{q^2(4-n)Z} \tag{21}$$

with

$$Z = W\left(\frac{\beta(1+q)}{q(4-n)} \cdot \exp\left\{\frac{\beta(1+q) - 2q\ln(m/\phi)}{q(4-n)}\right\}\right),$$

where $W(\cdot)$ is the Lambert function defined by the equation $W(s)\, e^{W(s)} = s$. It is a multivalued function with an infinite number of branches such that for each non-zero value of s there is an

infinite number values of W, most of them complex. Here the principal branch is used. The dependence of θ_f on m/ϕ is shown in Fig. 2 for $\beta = 10$, $q = 5$ for different values of n. Note that for all n, Eq. (21) ensures $\theta_f = 1$ for $m/\phi = 1$. At $m/\phi > 1$, the flame temperature, if the steady-state exists, always exceeds unity (the adiabatic temperature value) and the combustion process is superadiabatic.

The gas temperature distribution outside the porous layer is

$$\theta = \begin{cases} A_1 \exp(mx), & x < 0, \\ A_2, & x > \ell, \end{cases} \tag{22}$$

where A_1 and A_2 are unknown constants. Using this, Eqs. (10) allow to write the following conditions

$$\begin{aligned} x = 0: &\quad m\theta - \phi d\theta/dx = 0; \\ x = L: &\quad d\theta/dx = 0\,. \end{aligned} \tag{23}$$

The general solution on both sides of the flame-sheet becomes

$$\theta = \theta_s + \begin{cases} C_1 e^{a_1 x} + C_2 e^{a_2 x} & 0 < x < x_f\,, \\ C_3 e^{a_1 x} + C_4 e^{a_2 x} & x_f < x < \ell\,, \end{cases} \tag{24}$$

where

$$a_{1,2} = \frac{m \pm \sqrt{m^2 + 4\phi\, b}}{2\phi}\,.$$

An additional condition required to determine the solid phase temperature is given by Eq. (13). For time-independent cases, it takes the form

$$\theta_s = \frac{1}{\ell} \int_0^\ell \theta\, dx\,. \tag{25}$$

This means that, in the absence of heat losses, the temperature of the solid phase coincides with the gas temperature averaged within the porous layer.

Five conditions for the temperature field, namely Eqs. (16), (23) and (25), serve to determine the unknown values C_i, $i = 1 \ldots 4$ and θ_s. These equations are all linear with respect to these quantities. Despite the fact that these solutions are expressed in an analytical form, it makes no sense to write them down here because of their length. After finding them, analytical expressions for the gas temperature on both sides of the flame-sheet were substituted into

$$[d\theta/dx]_{x=x_f} + F(\theta_f) = 0. \tag{26}$$

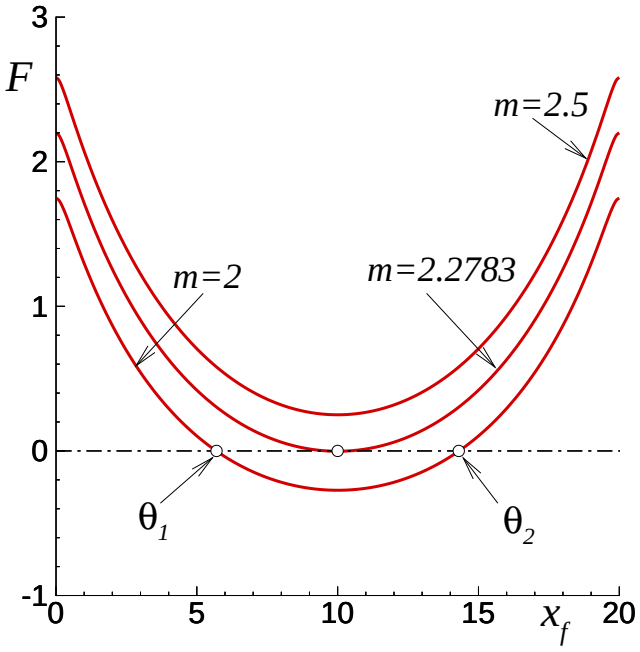

Figure 3: Typical dependencies of the function $\mathcal{F}$ on x_f for different values of m; all curves are plotted for $q = 5$, $\beta = 10$, $n = 2$, $\ell = 20$, $\phi = 0.4$, $b = 0.2$. The open circles for the curve with $m = 2$ correspond to the solutions drawn in Fig.4.

The last step allows to find the flame position x_f. All these procedures were carried out using MAPLE facilities.

Based on the procedure described above, we can conclude that the steady-state results obtained within the framework of the flame sheet model are independent of the Lewis number. First of all, Eq. (20) which determines the relationship between the flame temperature and the flow rate does not depend on the Lewis number. The Lewis number similarly does not appear in Eqs. (16), (23) and (25) required for finding C_i, $i = 1 \ldots 4$ and θ_s, all functions of θ_f. After finding analytical expressions for the temperature on both sides of the flame sheet, these expressions are substituted into Eq. (26), which as a consequence does not present a dependence on the Lewis number.

However, it should be noted that this independence of the results from the Lewis number, which expresses the ratio of diffusion to the thermal diffusivity of the gas, is the result of the adequate choice of the thermal flame width as a characteristic size of the problem. If the results are rewritten using dimensional variables, then they are clearly dependent on the fuel diffusion.

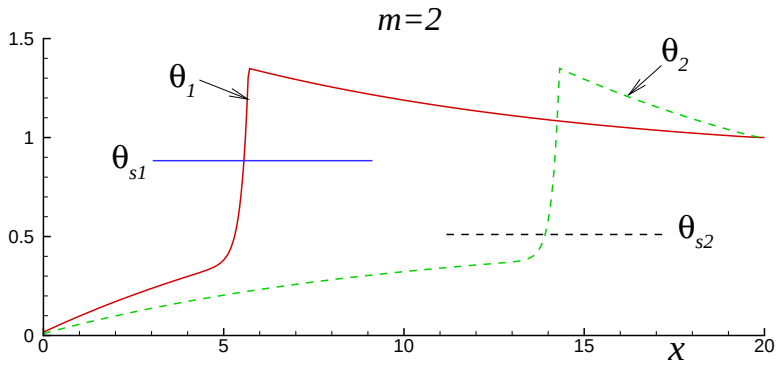

Figure 4: An example of temperature distributions (plotted within the porous layer only) for the lower (solid curve) and upper (dashed curve) solutions corresponding to the open circles on the curve with $m = 2$ in Fig. 3. Temperature values for the solid phase are indicated by horizontal lines.

The final analytical expression to determine x_f given by Eq. (26) (very long, also not represented here) takes the form

$$\mathcal{F}(x_f; m, \phi, b, N, q, n) = 0\,. \tag{27}$$

This nonlinear equation was used to evaluate x_f numerically. Figure 3 shows typical dependencies of the function $\mathcal{F}$ on x_f for various values of m with other parameters fixed. These curves illustrate that Eq. (27) can have two, one or zero roots.

Let's call the solutions corresponding to the lower and higher values of x_f as lower, $\theta_1(x)$, and upper, $\theta_2(x)$. These distributions are illustrated in Fig. 4 with solid and dashed lines, respectively. One can see that although both solutions correspond to the same value of θ_f (according to Eq. (20), it depends on m/ϕ only), the solid phase temperatures for these two solutions are different, $\theta_{s1} > \theta_{s2}$. These values are plotted in Fig. 4 with horizontal solid and dashed lines. Note also that for any steady-state solution the temperature at the exit from the porous layer is equal to unity, as it should be, since there are no heat losses.

Figure 5 illustrates typical dependencies of the flame position x_f (left plot) and the solid phase temperature θ_s (right plot) as functions of the dimensionless gas flow rate m. The response curves are shown for $n = 0, 1$ and 2. All other parameters are fixed at $\beta = 10$, $q = 5$, $\ell = 20$, $b = 0.2$ and two values of ϕ. It can be seen that the curves have a familiar C-shape. When the flow intensity approaches the critical value $m = m_c$, the two solutions merge and disappear at $m > m_c$. One can see that the influence of the parameter n is only moderately quantitative, leading to a decrease in the critical value, m_c, with increasing n.

Figure 3 shows that when two roots merge into one, at $m = m_c$, the function $\mathcal{F}(x_f, m, \dots)$

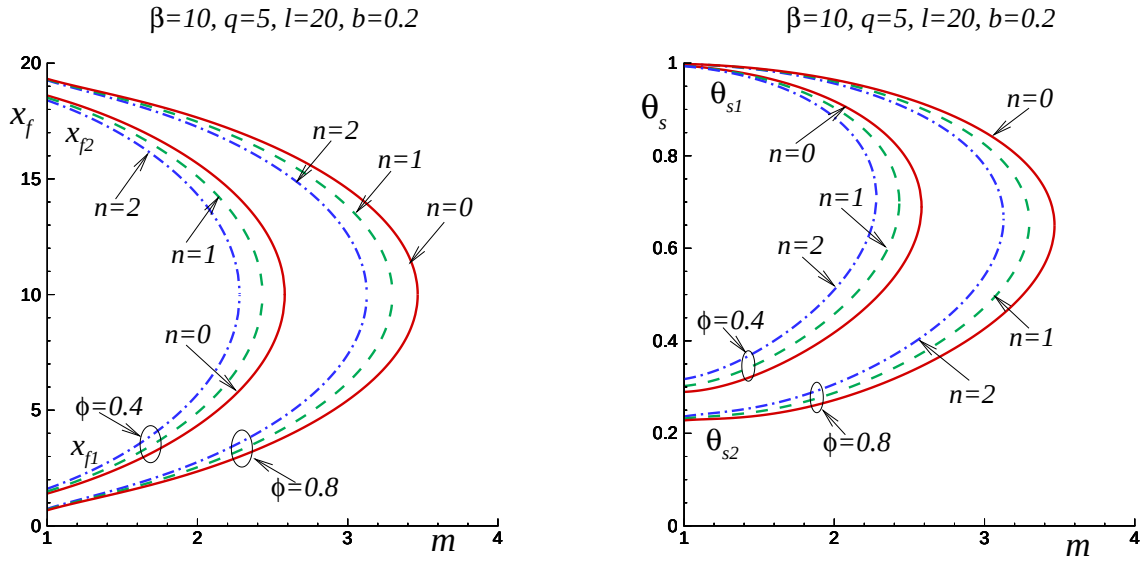

Figure 5: Typical dependencies of the flame position x_f (left plot) and solid phase temperature θ_s (right plot) on the flow rate for $n = 0$, 1 and 2.

becomes tangent to the horizontal axis. A rigorous determination of the critical values requires to solve a system of two equations with respect to x_f and m,

$$\mathcal{F}(x_f, m, \dots) = 0, \quad \frac{\partial \mathcal{F}}{\partial x_f}(x_f, m, \dots) = 0\,. \tag{28}$$

It was obtained that for $m = m_c$ the critical flame position is situated exactly in the middle of the porous layer, namely $x_f = \ell/2$ always takes place.

The existence of an analytical expression given by Eq. (27) facilitates greatly the parametric analysis of the solutions. Figure 6 illustrates the dependence of the critical value of the flow rate on the heat release parameter q (left plot) and on the porosity value (right plot) for layers with different ℓ. Note that the dimensionless activation energy N is fixed in the left figure, and not the Zel'dovich number calculated according to $\beta = Nq/(1+q)^2$. It can be seen that with increasing q (which leads to a decrease in β), the critical value for the flow rate decreases. If the layer width ℓ increases, as can be seen in the right plot, the value of the critical flow rate increases.

Figure 7 illustrates the dependence of the critical flow rate, m_c, on the dimensionless heat exchange value between phases, b, for two porous layer widths and various n. As expected, an increase in the heat transfer leads to an increase in m_c.

The above dependencies show that the effect of heat recirculation, which increases the maximum flow rate below which there are steady-state regimes, grows monotonically with an increase in the thickness of the porous layer, with an increase in the efficiency of heat exchange

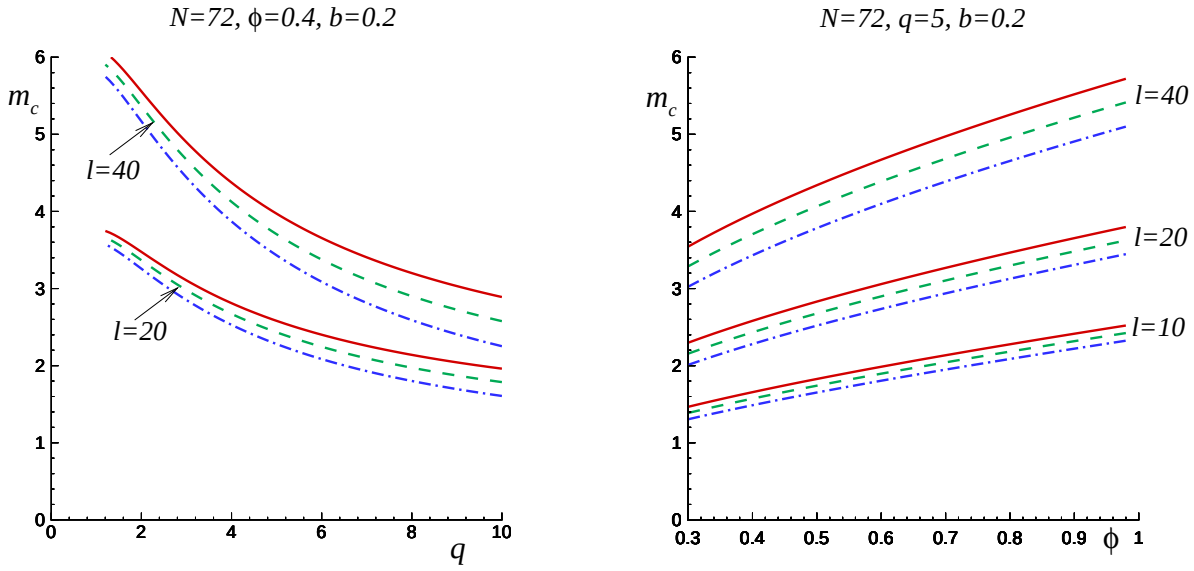

Figure 6: Dependencies of the critical value for the flow rate, m_c, on the heat release q (left plot) and the porosity ϕ (right plot) for various values of the parameters; the solid, dashed and dash-dotted lines correspond to $n = 0$, 1, and 2, respectively.

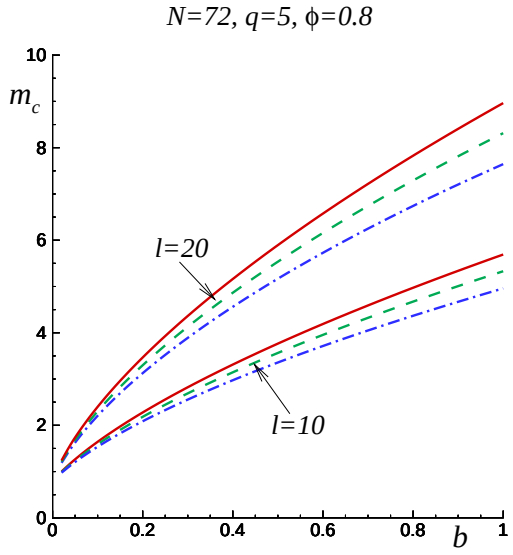

Figure 7: Dependencies of the critical value for the flow rate, m_c, on the heat exchange coefficient b for various values of the parameters; the solid, dashed and dash-dotted lines correspond to $n = 0$, 1, and 2, respectively; all curves plotted for $\phi = 0.8$.

between the gas and solid phases or with an increase in the porosity. However, an increase in thermal expansion q leads to a decrease of the maximum flow rate. It should be remembered

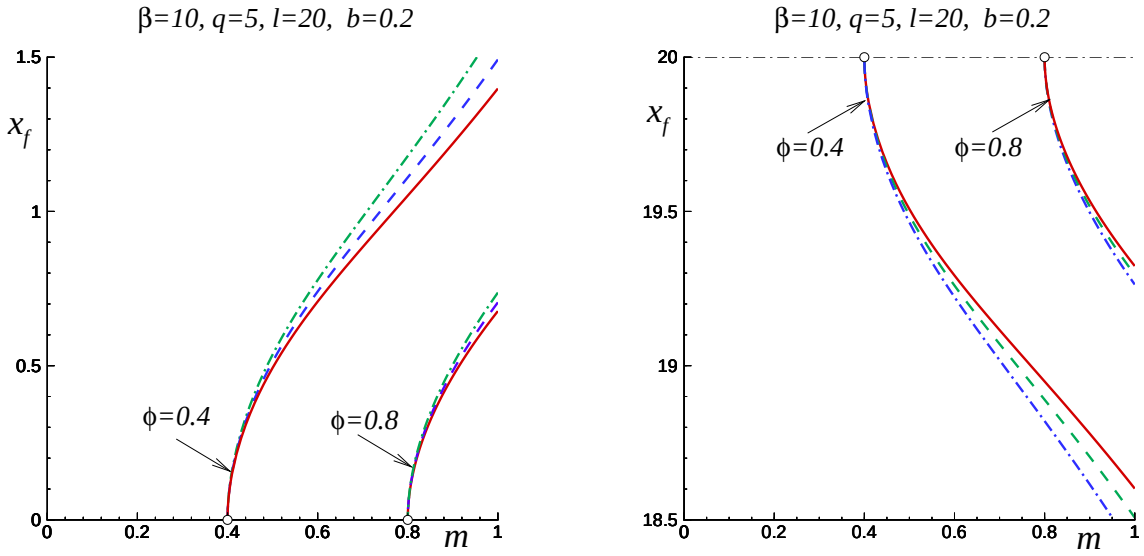

Figure 8: Flame position as a function of m for $\phi < m < 1$ for the lower (left plot) and upper (right plot) branches plotted for $\phi = 0.4$ and 0.8; the solid, dashed and dash-dotted lines correspond to $n = 0$, 1, and 2, respectively.

that the flame temperature, θ_f, which depends only on the flow rate divided by the porosity coefficient, see Eq. (20), always exceeds the adiabatic temperature of the mixture in these cases.

3.4 Effect of flame stabilization by a porous layer

For all the cases presented above, the upstream gas flow rate was chosen to be greater than the planar flame propagation speed, $m = U_0/S_L \geqslant 1$. Obviously, for these cases, upstream flame propagation does not occur. However, if ignition takes place at $x > \ell$, then there is a time-dependent solution in the form of a combustion wave propagating downstream at a speed $v = m - 1$ relative to the porous layer. In the same way, when the dimensionless flow rate is less than one, $m < 1$, there is also a time-dependent solution of Eqs.(3)-(6) describing the combustion wave propagation towards negative x with a negative speed, $v = m - 1$.

A parametric analysis of Eq. (27) showed that for $m < 1$, in addition to the solutions in the form of a traveling wave, there are also steady-state solutions with the flame position located inside the porous layer. Figure 8 shows the dependence of x_f on the flow rate for the lower (left plot) and upper (right plot) solutions drawn for two values of $\phi = 0.4$ and 0.8 and values of $n = 0$, 1 and 2. It can be seen that, regardless of n , the critical value m_* at which the position of the flame is situated at $x_f = 0$ or $x_f = \ell$ is equal to ϕ. In both cases, $\theta_f = 1$, as follows

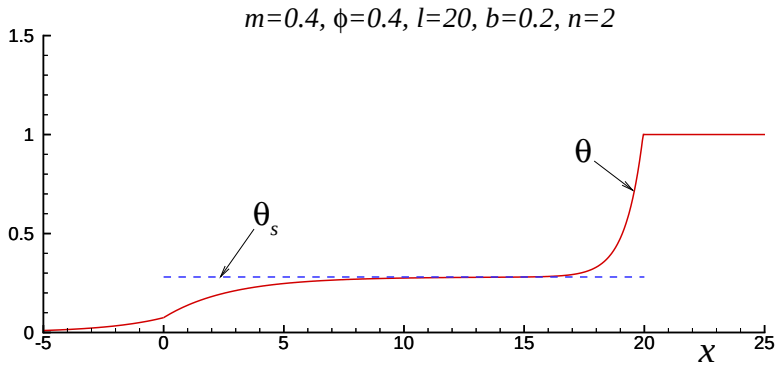

Figure 9: The limiting solution with the flame located at $x_f = \ell$; for $m = 0.4$, $\phi = 0.4$, $\ell = 20$, $n = 2$ and $b = 0.2$; the solid phase temperature is $\theta_s \approx 0.2804$.

from Eq (20). The same behavior for the response curves was observed for other values of the parameters.

The limiting solution with the flame position at $x_f = 0$ is trivial,

$$\theta = \begin{cases} e^x, & x < 0\,, \\ 1, & x > 0\,, \end{cases} \qquad \theta_s = 1\,. \tag{29}$$

This can be easily verified by substituting Eq. (29) into the governing equations. Obviously, this solution is independent of other parameters. The temperature of the solid phase is exactly equal to the temperature of the gas behind the combustion zone.

For the other solution corresponding to the flame situated at $x_f = \ell$, an example of temperature distributions in the gas and solid phases is shown in Fig. 9 plotted for $m = 0.4$, $\phi = 0.4$, $\ell = 20$, $b = 0.2$. In this case, the solid phase is heated to a certain temperature less than the temperature behind the combustion zone, which is also equal to unity. The gas temperature is less than θ_s at the beginning of the porous layer and exceeds θ_s at the end of the layer. The value of the temperature of the solid phase depends on the parameters. Anticipating the results of time-dependent simulations, the upper branch solutions (corresponding to $\ell/2 < x_f < \ell$) result to be unstable. However, the temperature distribution shown in Fig. 9 represents the asymptotic solution for the third steady-state mode described below, see also Appendix, when the flame is located at the trailing edge of the porous layer. This solution is stable.

Although this effect can be explained by an increase of the local gas velocity between the pores (due to a decrease in the average free area), it is interesting that the critical value of the gas flow rate for flame stabilization, $m_c = \phi$, does not depend on other parameters such as b, for example, within the framework of the model under study. In this case, the temperatures of

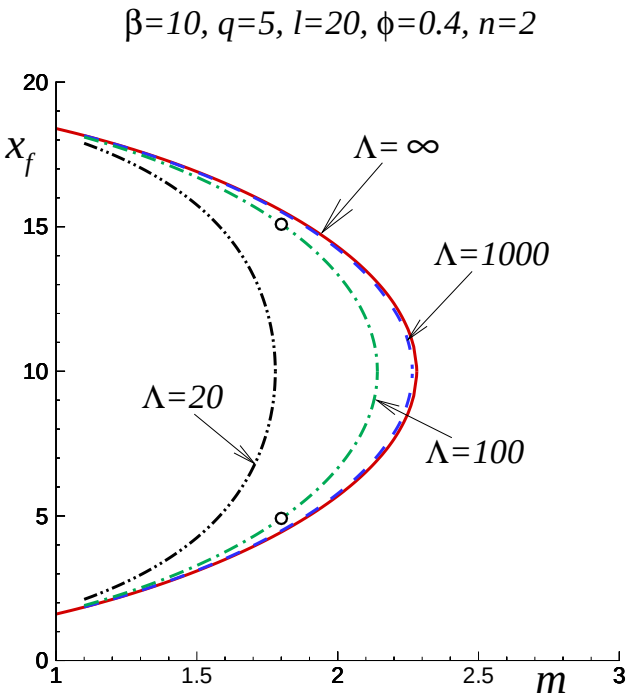

Figure 10: Comparison of response curves obtained for different Λ values.

the gas and the porous medium are different for the solutions with $\phi < m < 1$ and the heat exchange term is not equal to zero. Apparently, flame stabilization by a porous layer of finite length has not been considered by other authors in previous studies.

Note that in order to search for possible steady-state solutions with a flame located at $x_f < 0$ or $x_f > \ell$, it is necessary to replace Eq. (20) with $F(\theta_f) = m$. The rest of the steps presented above remain practically the same. This was done, but no steady-state solutions corresponding to $x_f < 0$ or $x_f > \ell$, namely roots of Eq. (27), were found. This issue will be discussed when comparing the results obtained in the framework of the flame sheet model and those with a finite flame width. The $x_f = \ell$ case is discussed also in the Appendix within the flame sheet model.

3.5 Comparison with finite Λ solutions

It is interesting to compare the solutions obtained for infinite Λ with those for finite Λ values. This type of solutions was recently investigated in [17]. The comparison also ensures the validation of the asymptotic results reported above. For this, Eqs. (4) and (5) were solved together with Eq. (6) within the flame sheet model. Note that the temperature of the solid phase depends on x in these cases.

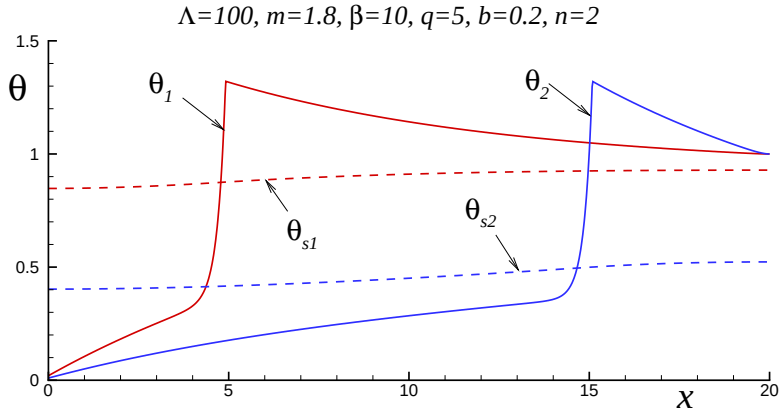

Figure 11: The temperature distributions obtained within the flame-sheet model at $\Lambda = 100$ and $m = 1.8$ corresponding to the open circles in Fig. 10

The mass fraction solution given by Eq. (19) remains the same for the case of finite Λ. The general solution for the temperatures of the gas and the solid phase was obtained in analytical form. This solution has a much longer form than for $\Lambda \gg 1$, and is also not presented here. The roots of the final algebraic expression equivalent to Eq. (27) determining the flame position x_f were investigated numerically.

Figure 10 shows the response curves calculated for $\Lambda = 20$, 100 and 1000 drawn using dash-dot-dot, dash-dot and dashed lines, respectively. The solid line represents the case with $\Lambda \to \infty$. It can be seen that with a gradual increase in Λ, the response curve approaches the limit curve for infinite Λ. This result is explained by the fact that the maximum effect of heat recirculation is obviously achieved at $\Lambda \to \infty$. The solutions indicated by open circles on the curve with $\Lambda = 100$ are illustrated in Fig. 11.

4 Numerical solutions for β finite

In order to complete the validation of the analytical results presented above, the analytical solutions are compared with the solutions obtained numerically for the distributed reaction rate. These simulations were performed for various parameter values. Comparison is presented for selected values only. For other values, this procedure gives similar results. As explained in section 3.3, the Lewis number falls out of the parameters in the flame-sheet model. The numerical calculations presented below were carried out for $Le = 1$.

4.1 Numerical treatment

Steady as well as time-dependent computations were carried out in a finite domain, $x_{min} < x < x_{max}$. The typical values were $x_{min} = -10$ and $x_{max} = \ell + 10$, but they were also varied to ensure the independence of the results. The spatial derivatives were discretized using second-order, three-point central finite differences on a rectangular uniform grid. The number of grid points varied from 2001 to 5001. Control calculations with a doubled number of grid points were carried out in the same way without finding noticeable changes in the results.

The steady-state solutions were obtained using two iterating methods, in both applying a Gauss-Seidel procedure with over-relaxation. In the first method, the value of the flow rate, m, was fixed. Only solutions belonging to the stable branch (see below) can be calculated using this method. In the second method, the temperature was fixed at a point with $x = x_*$ imposing there $\theta = \theta_*$ while the value of m was calculated iteratively (also with a Gauss-Seidel procedure).

For stable branches of the response curve, both methods give the same results (as they should). However, it should be noted that, when calculating unstable branches, the (second) iterative method became very stiff and slow when approaching the turning point appearing near $x \lesssim \ell$ (see below). In these cases, taking into account the continuity of the response curves, the turning point was identified approximately by interpolating (only in Fig. 13).

For unsteady calculations an explicit marching procedure with first order discretization in time was used. The presence of the highly nonlinear reaction rate term requires to choose the time step, τ, sufficiently small. The typical value was $\tau = 10^{-5} \div 10^{-6}$. No significant differences were found in the results when τ was halved.

4.2 Steady-state results

Figure 12 compares for $n = 0$ and $n = 2$ the response curves plotted for $m \geqslant 1$ obtained in the framework of the flame sheet model (solid and dashed lines) and those calculated for the distributed reaction rates (triangles and open circles symbols). The curves with $n = 1$ lie between these cases and are not shown in order not to overload the figure. It can also be seen that taking into account the dependence on the index n in Eq. (15) thus reflecting the reaction rate dependence on the density strongly contributes to the coincidence of the curves. One can see good agreement between the results for $\beta = 10$ obtained with the two models, one with an infinitely thin reaction rate and the other with a distributed reaction rate, and perfect agreement for higher β values.

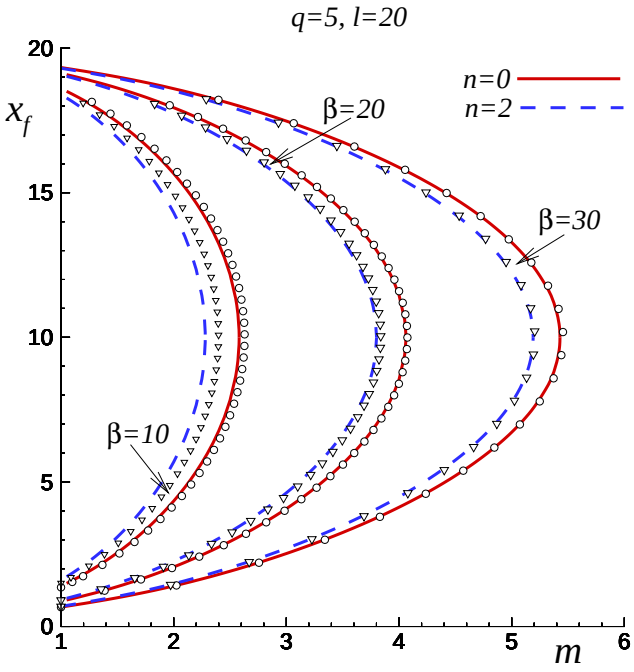

Figure 12: Comparison of the response curves for the flame position versus flow rate obtained within the flame sheet model (solid lines - $n = 0$, dashed lines - $n = 2$) and from numerical calculations at finite β (triangular symbols - $n = 2$, open circles - $n = 0$); for $\ell = 20$, $q = 5$, $b = 0.2$ and $\phi = 0.4$.

The complete response curve for all m is illustrated in Fig. 13 for $\beta = 10$, $q = 5$, $\ell = 20$, $b = 0.2$, $\phi = 0.4$ and $n = 2$. It can be seen that for $m < 1$, in addition to the two solutions reported before, a third solution appears for which the flame is located near $x = \ell$. As the flow rate approaches one on the left side along this branch, $m \to 1-$, the flame position x_f increases, namely the flame moves away from the porous surface. As mentioned above, the numerical calculation of a relatively small part of the response curve in the intermediate branch turned out to be difficult, and this interval is drawn with a dashed line segment in Fig. 13. The temperature and mass fraction distributions for the solutions corresponding to open triangle symbols in Fig. 13 are shown in Fig. 14 for $m \approx 0.973$. It can be seen in Fig. 14 that for the two solutions shown in the two upper plots, with the flame located inside the porous layer, the maximum temperature exceeds the adiabatic value, while this does not happen for the solution with the flame located at the rear boundary of the porous layer shown in the bottom plot. In a sense, the last solution resembles the situation studied in [18–21]. However, the important

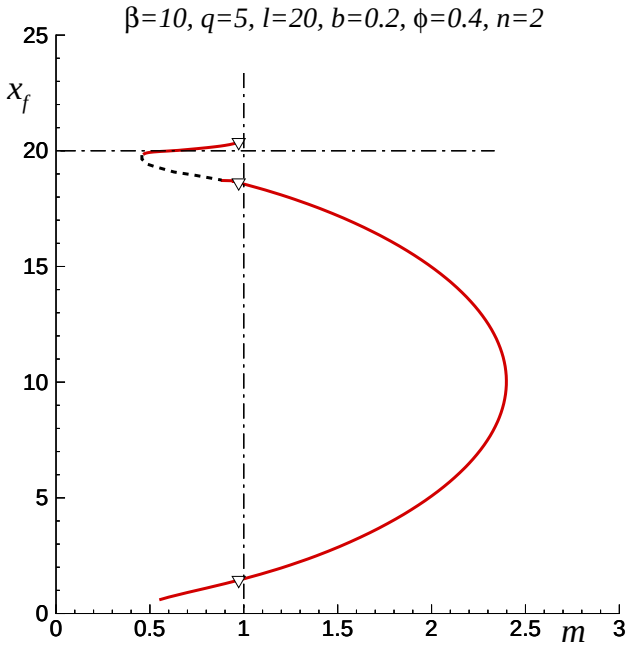

Figure 13: Response curve for the case with a spatially distributed reaction zone, for $\beta = 10$, $q = 5$, $\ell = 20$, $b = 0.2$ and $\phi = 0.4$; open triangles correspond to the distributions shown in Fig. 14.

difference is that the temperature of the porous medium is not fixed. As a consequence, the porous solid is heated and the flame can approach the rear boundary of the solid. A discussion of the third type solutions within the framework of the flame sheet model is given in the Appendix.

Figure 15 illustrates the behavior of solutions near the front and back ends of the porous layer plotting x_f versus m. The left plot shows the behavior of the response curves near $x = \ell$ for the flame sheet and the distributed reaction models. The solid line shows the response curve obtained within the flame sheet model for $\beta = 10$ and $q = 5$, $\ell = 20$, $b = 0.2$, $\phi = 0.4$, $n = 2$. The curves calculated using the distributed reaction rate for $\beta = 10$, 20 and 30 are plotted with dashed, dash-dot and dash-dot-dot lines, respectively, with the same set of other parameters. All these curves belong to the third family of solutions. One can see that with the increase in β (the width of the reaction zone is decreasing), the curves approach the line $x_f = \ell$. The position of the turning point, m_*, depends on β and approaches the limiting value $m_* = \phi$ as β grows. The solid horizontal line in Fig. 15 (left) indicates the limiting behavior for $\beta \gg 1$ discussed in the Appendix.

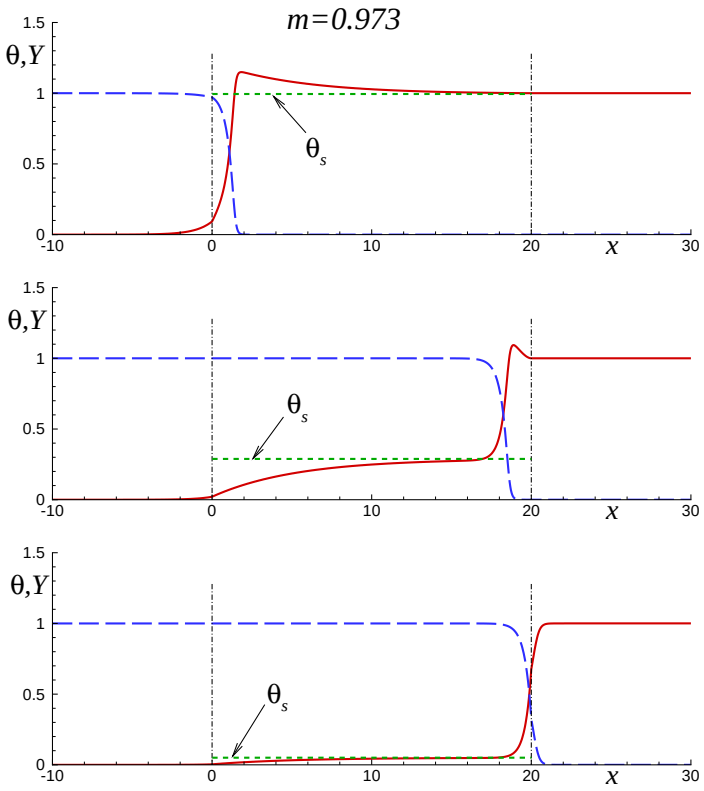

Figure 14: The gas and solid temperatures (solid and dashed lines), and mass fraction distributions (long dashed lines) for the three solutions corresponding to the open triangles in Fig. 13 for $m = 0.973$.

The right plot of Fig. 15 shows the behavior of the lower solution with decreasing values of the flow rate. The solid lines correspond to the flame sheet model while the dashed and dashed-dot lines correspond to the distributed reaction zone model. It can be seen that the dashed and dashed-dot curves are interrupted at values of m greater than ϕ. For example, for the parameters used in the figure, the critical value of the flow rate is $m_* \approx 0.51$ for $\beta = 10$. No steady-state solutions were found for smaller m. Thus, all this shows the dependence of the critical value of the flow rate on the Zel'dovich number; nevertheless, m_* tends to the limiting value $m_* = \phi$ with decreasing in width of the reaction rate region.

4.3 Time-dependent solutions

In order to investigate the stability of the above solutions, time-dependent simulations were performed. For this, the initial conditions in the form of a planar combustion wave located in

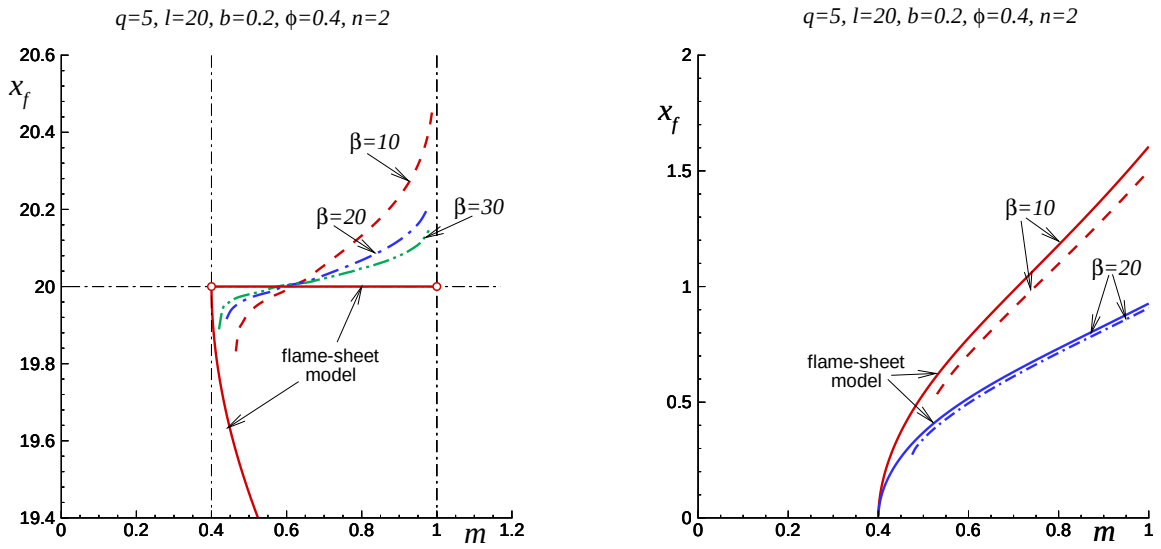

Figure 15: Response curves for the upper (left plot) and lower (right plot) solutions. The flame-sheet curve (solid line) in the left plot is drawn for $\beta = 10$ only.

front of, or behind, the porous layer were first used. Figure 16 gives time histories of the flame position for different cases.

It can be seen in Fig. 16 that for $m = 0.8$ and 0.35, when the initial position of the combustion zone was chosen behind the porous layer, the flame propagated upstream at a constant velocity. After a transitional period, the solution with $m = 0.8$ turned into a steady-state solution corresponding to the combustion regime situated near the porous layer edge, $x_f \approx \ell$. For the case with $m = 0.35$, the flame went through the porous layer and continued to spread upstream, as it should have been, since $m = 0.35$ is less than the critical value. For the case $m = 1.5$, an initial position of the combustion zone ahead the porous layer is chosen. It can be seen that the lower flame regime is established after a transition period.

The stability for the intermediate regime with the combustion zone located in the back half of the layer was also tested. For this, the steady-state intermediate solution with $m = 0.973$ was first computed and small perturbations of this state were introduced in the temperature field. These distributions were then used as an initial condition for time-dependent modeling. The results are presented in Fig. 17, which shows the time histories for the flame position for two cases.

It can be seen that, for two small but different perturbations, the flame dynamics develops in two directions. In one case, the flame moves upstream and establishes inside the porous layer

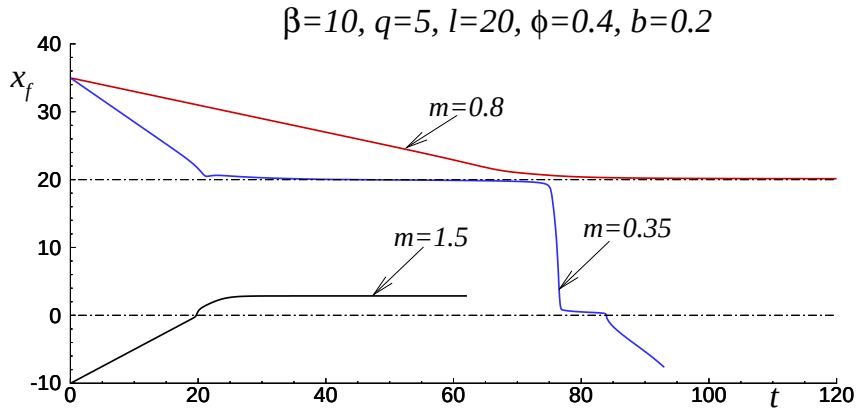

Figure 16: Flame position histories for ignition downstream of the porous layer (cases with $m = 0.8$ and 0.35) and upstream of the porous layer (curve with $m = 1.5$).

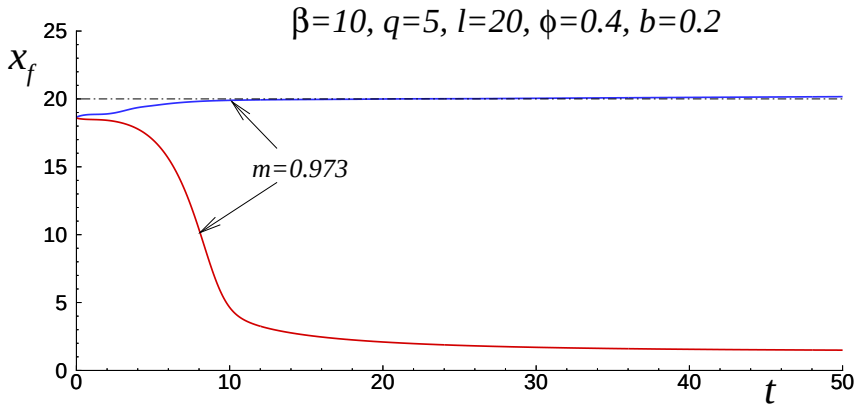

Figure 17: Flame position histories with two initial states obtained by small perturbations of the intermediate steady-state solution.

(lower regime). In the other case, the flame moves downstream and approaches the third steady solution situated at $x_f \approx \ell$. These two solutions are therefore stable and the initial intermediate solution with $x_f \approx 19$ for $m = 0.973$ corresponding to the middle plot in Fig. 14 is unstable.

Thus, one can conclude that when there are two possible modes (for $m > 1$), the upper mode is unstable while the lower one is stable. In the case of three solutions (for $m_* < m < 1$), the intermediate regime results unstable and the other two solutions are stable. In the last case, the actual establishment of one or the other flame mode depends on the initial conditions.

It should be noted that when the flame is attached to the rear boundary of the porous layer the combustion regime differs from those considered in [18–21]. In those studies, the flow rates were also less than the planar flame velocity. However, the temperature of the porous plug was kept constant and cold. Thus, the flame could not approach the edge of the porous layer and was

stabilized at a finite distance from it.

5 Conclusions

The main feature of combustion devices in which a super adiabatic temperature is achieved is the preheating of a fresh cold initial mixture entering the device using heat from hot combustion products leaving this device. Importantly, this preheating procedure does not require additional costs and makes it possible to maintain a stable combustion process. However, it is obvious that this mode of operation can be realized only at certain values of the parameters, which are determined by the properties of the materials from which the device is made, and the properties of the burning mixture itself.

The phenomenon of multiplicity of steady-state regimes is apparently common to superadiabatic devices. In all devices of this type, it turns out that both stable and unstable modes of operation exist simultaneously. For this reason, determining the parametric range where the different regimes exist is an important ingredient in the analysis.

When investigating the operation of combustion devices, the number of parameters describing the system is usually quite large. This can create difficulties for parametric analysis. In this regard, simplified models that allow analytical analysis are an excellent guide to device design.

One of the possible designs for such super adiabatic devices is a channel system in which the burning mixture flows in a countercurrent manner for adjacent channels. In this case, the thickness of the channels should be small to improve the heat transfer between them, which possibly imposes restrictions related to the throughput of the system. Another option is an inert porous layer through which the mixture flows. In this case, these possible restrictions can be relaxed. This is the type of devices studied in the present work.

The key tool in the presented analysis is the use of the flame sheet model, in which, however, the dependence of the reaction rate on the density of the mixture was taken into account. It should be noted that this has not been done in previous studies. The proposed method made it possible to write down solutions in an analytical form, which greatly simplified the parametric analysis of the problem.

As mentioned above, the study of the multiplicity of modes of operation was the main task. It turned out that, apart from the cases where only two regimes take place, there is a parameter range within which three non-trivial steady-state modes can be realized simultaneously. The latter possibility has not been previously considered in the literature. Finally, it should be noted

that the validity of the analysis carried out at the limiting values is well supported by numerical results carried out for finite values of the parameters.

Acknowledgment

This paper is part of project #PID2019-108592RB-C42 funded by
MCIN/AEI/10.13039/501100011033.

Appendix

As indicated in Sec. 3.4, the analytical procedure carried out using $\omega \sim \delta(x-x_f)$ for the reaction rate reveals the absence of steady-state solutions with $x_f < 0$ or $x_f > \ell$. It turns out that the above flame sheet model fails to describe the third solution appearing for $m < 1$ with the flame position located at $x_f \approx \ell$. This can be explained as follows.

When formulating the problem, it was assumed that the porosity dependence, $\Phi(x)$, is given by a step function with discontinuities at $x = 0$ and $x = \ell$. Obviously, this shape creates difficulties when using the δ-function as the reaction rate.

Suppose that instead the function $\Phi(x)$ is continuous near the ends of the interval $0 < x < \ell$, as shown in Fig. 18 where a continuous (e.g. linear) transition from $\Phi = 1$ to $\Phi = \phi$ is ensured using small intervals of width σ in x. For such a function, instead of Eq. (20), we get

$$m = \Phi(x_f) \cdot F(\theta_f)$$

obtained after integrating the mass fraction equation. The solution of the problem with this linear and continuous function $\Phi(x)$ can be constructed in an analytical form. However, one can understand the flame structure avoiding complex formulae.

Indeed, when the flame is located near the right edge of the porous layer, the flame temperature should be close to unity, $\theta_f \approx 1$, because the temperature value is equal to unity for $x > \ell$. The flame position, x_f, located within the narrow σ-interval near the edge of the porous layer is determined by equation $m = \Phi(x_f)$. Considering $\sigma \ll 1$, it can be obtained that, within the framework of the flame sheet model, the corresponding solutions in the plane x_f versus m are represented by segment $\phi < m < 1$, $x_f \approx \ell$. It is showed with a solid horizontal line in Fig.15 (left). For $\sigma \ll 1$, the temperature distributions for $\phi < m < 1$ are close to that plotted in Fig. 9.

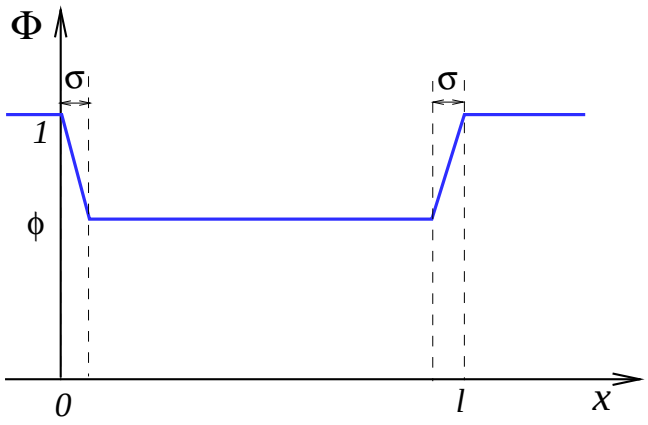

Figure 18: Continuous porosity sketch.

References

[1] S.A. Lloyd, F.J. Weinberg, A burner for mixtures of very low heat content, *Nature* 251 (1974) 47-49.

[2] S.A. Lloyd, F.J. Weinberg, Limits to energy release and utilisation from chemical fuels, *Nature* 257 (1975) 367-370.

[3] A.R. Jones, S.A. Lloyd, F.J. Weinberg, Combustion in heat exchangers, *Proc. R. Soc. Lond. A.* 360 (1978) 97-115.

[4] A.C. Fernández-Pello, Micropower generation using combustion: issues and approaches, *Proc. Combust. Inst.* 29 (2002) 883-899.

[5] D. Dunn-Rankin, E.M. Leal , D.C. Walther, Personal power systems, *Prog. Energy Combust. Sci.* 31 (2005) 422-465.

[6] S. Wood, A.T. Harris, Porous burners for lean-burn applications, *Prog. Energy Combust. Sci.* 34 (2008) 667-684.

[7] Y. Ju, K. Maruta, Microscale combustion: technology development and fundamental research, *Prog. Energy Combust. Sci.* 37 (2011) 669-715 .

[8] D.C. Walther, J. Ahn, Advances and challenges in the development of power-generation systems at small scales, *Prog. Energy Combust. Sci.* 37 (2011) 583-610 .

[9] K. Maruta, Micro and mesoscale combustion, *Proc. Combust. Inst.* 33 (2011) 125-150.

[10] N.S. Kaisare, D.G. Vlachos, A review on microcombustion: fundamentals, devices and applications, *Prog. Energy Combust. Sci.* 38 (2012) 321-359.

[11] J.L. Ellzey, E.L. Belmont, C.H. Smith, Heat recirculating reactors: Fundamental research and applications, *Prog. Energy Combust. Sci.* 72 (2019) 32-58.

[12] T. Takeno, K. Sato, An excess enthalpy flame theory, *Combust. Sci. Tech.* 20 (1979) 73-84.

[13] B. Deshaies, G. Joulin, Asymptotic study of an excess-enthalpy flame, *Combust. Sci. Tech.* 22 (1980) 281-285.

[14] F.M. Pereira, A.A.M. Olivera, F.F. Fachini, Asymptotic analysis of stationary adiabatic premixed flames in porous inert media, *Combust. Flame* 156 (2009) 152-165.

[15] F.M. Pereira, A.A.M. Olivera, F.F. Fachini, Theoretical analysis of ultra-lean premixed flames in porous inert media, *J. Fluid. Mech.* 657 (2010) 285-307.

[16] F.M. Pereira, A.A.M. Olivera, F.F. Fachini, Maximum superadiabatic temperature for stabilized flames within porous inert media, *Combust. Flame* 158 (2011) 2283-2288.

[17] P.-A. Masset, O. Dounia, L. Selle, Fully explicit formulae for flame speed in infinite and finite porous media, *Combust. Theory Modell.* 25 (2021) 785-812.

[18] G. Joulin, Conductive interactions of a wrinkled flame with a cold flat burner, *Combust. Sci. Technol.* 27 (1981) 83-86.

[19] G. Joulin, Flame oscillations induced by conductive losses to a flat burner, *Combust. Flame* 46 (1982) 271-282.

[20] V.N. Kurdyumov, M. Matalon, The porous-plug burner: Flame stabilization, onset of oscillation, and restabilization, *Combust. Flame.* 153 (2008) 105118.

[21] V.N. Kurdyumov, M. Mario Sánchez-Sanz, Influence of radiation losses on the stability of premixed flames on a porous-plug burner, *Proc. Combust. Inst.* 34 (2013) 989-996.

[22] J. Buckmaster, T. Takeno, Blow-off and flashback of an excess enthalpy flame, *Combust. Sci. Tech.* 25 (1981) 153-158.

[23] T. Takeno, K. Sato, K. Hase, A theoretical study on an excess enthalpy flame, *Proc. Combust. Inst.* 18 (1981) 465-472.

[24] D.J. Diamantis, E. Mastorakos, D.A. Goussis, Simulations of premixed combustion in porous media, *Combust. Theory Modell.* 6 (2002) 383-411.

[25] R. Fursenko, A. Maznoy, E. Odintsov, A. Kirdyashkin, S. Minaev, K. Sudarshan, Temperature and radiative characteristics of cylindrical porous NiAl burners, *Int. J. Heat Mass Tranfer* 98 (2016) 277-284.

[26] D.A. Nield, A. Bejar, Convestion in porous media, Springer, 2006.

[27] J.C. Graña-Otero , Nonlinar dynamics of unsteady premixed, planar flames, Universidad Politécnica de Madrid, 2009, Doctoral thesis (under the direction of Dr. Amable Liñán).

[28] V.N. Kurdyumov, Propagation of premixed isobaric flames in narrow channels with heat-losses: The asymptotic analysis revised and reliance on the flame-sheet model, *Combust. Flame.* 206 (2019) 138-149.

[29] A. Liñán, The asymptotic structure of counterflow diffusion flames for large activation energies, *Acta Asronautica*, 1 (1974) 1007-1039.

[30] X. Fu, R. Viskanta, J.P. Gore, Measurement and correlation of volumetric heat transfer coecients of cellular ceramics, *Exp. Thermal Fluid Sci* 1998 (17) 285-293.

[31] W.B. Bush , F.E. Fendell, Asymptotic analysis of laminar flame propagation for general lewis number, *Combust. Sci. Technol.* 1 (1970) 421428.